FOUNDATIONS
ADVANCES

Volume 77 (2021)

Supporting information for article:

On single-crystal total scattering data reduction and correction protocols for analysis in direct space

Robert J. Koch, Nikolaj Roth, Yiu Liu, Oleh Ivashko, Ann-Christin Dippel, Cedomir Petrovic, Bo B. Iversen, Martin v. Zimmermann and Emil S. Bozin

Supporting information for "On single crystal total scattering data reduction and correction protocols for analysis in direct space"

Robert J. Koch,[a] Nikolaj Roth,[b] Yiu Liu,[a] Oleh Ivashko,[c] Ann-Christin Dippel,[c] Cedomir Petrovic,[a] Bo B. Iversen,[b] Martin v. Zimmermann[c] and Emil S. Bozin [a]*

[a]*Condensed Matter Physics and Materials Science Division, Brookhaven National Laboratory, Upton, NY 11973, USA,* [b]*Center for Materials Crystallography, Department of Chemistry and iNANO, Aarhus University, DK-8000, Aarhus, Denmark, and* [c]*Deutsches Elektronen-Synchrotron DESY, 22607 Hamburg, Germany. E-mail: bozin@bnl.gov*

1. Bragg Peak Width

A key aspect of the 3D-ΔPDF data reduction is removal of the Bragg peaks such that only a non-Bragg signal remains. This can be hindered if the instrumental resolution is poor, or Bragg peak width is large enough that adjacent Bragg peak tails overlap significantly.

To quantify the instrumental resolution in our experiment, we have fit a subset of the reconstructed reciprocal space data without dynamic masking. We have elected to focus on a Q_x line scan at $Q_y = Q_z = 0$ Å^{-1} for positive values of Q_x. The fit is composed of a sum of six pseudo-Voigt functions, where we have refined the peak position, the peak amplitude (area), fraction Lorentzian character (η), and the full-width at half-maximum (FWHM). The FWHM and peak position of the Gaussian and Lorentzian contributions to each individual pseudo-Voigt peak have been constrained to be identical. We have also included a sixth order polynomial to fit the background.

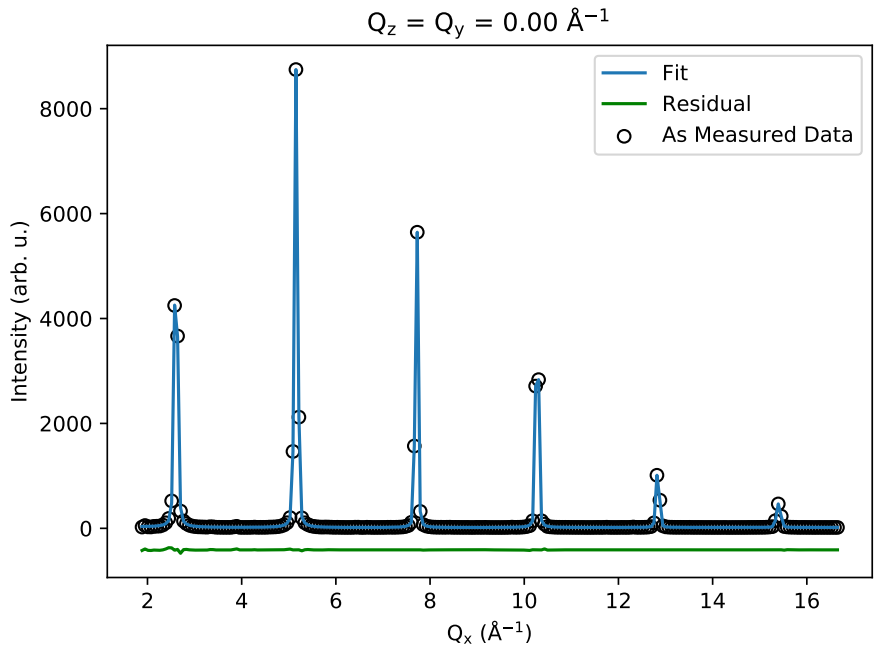

Fig. S1. A Q_x line scan of the reciprocal space intensity distribution (open black circles) after reconstruction from detector space without dynamic masking. The $Q_y = Q_z = 0$ Å^{-1} cut is shown for positive values of Q_x. Data have been fit (solid blue line) with six pseudo-Voigt profiles as described in the text. The fit residual (solid green line) is displaced vertically for clarity. Fitted parameters are presented in Table 1

The experimental data, fit, and fit residual are shown in Fig. S1. It is difficult to discern by eye any diffuse signal in this line scan, but the described fitting approach well reproduces the Bragg peaks. The refined set of peak parameters for this fit are

shown in Table 1. The peak FWHM and η remain within the ranges of 0.06-0.09 Å^{-1} and 0.2-0.4, respectively, suggesting that there is not a strong trend in peak shape as a function of Q_x.

Table 1. *Peak position, full-width at half-maximum (FWHM), fraction Lorentzian character (η), and peak amplitude extracted from fitting the reconstructed diffraction data without dynamic masking, as shown in Fig. S1 and described in the text. Refined uncertainties on the last digit are shown in parentheses.*

Position (Å^{-1})	FWHM (Å^{-1})	η	Amplitude (Å^{-1})
2.60441(9)	0.083(1)	0.39(2)	602(3)
5.15635(7)	0.0791(1)	0.304(8)	822(2)
7.7142(2)	0.0665(6)	0.24(2)	493(2)
10.2736(1)	0.063(9)	0.29(5)	410(20)
12.8371(7)	0.079(3)	0.23(7)	108(2)
15.402(1)	0.093(2)	0.2(1)	54(2)

As the goal of the 3D-ΔPDF experiment is accurate measurement of the diffuse intensity, and this diffuse intensity is often much weaker than the Bragg features, frame exposure times are chosen such that Bragg peaks often exceed the dynamic range of the detector. Practically this means that accurate Bragg peak intensities are often not present in either the detector images or the associated reconstructed reciprocal space intensity distribution. Saturated detector pixels only provide a only lower limits on the Bragg intensities. Without accurate Bragg peak intensities, one cannot estimate the true peak FWHM, one can only estimate an upper limit on the FWHM. The FWHM then as shown in Table 1 represent only our best estimate at the upper limit on the FWHM for the Bragg peaks in this configuration.

For a Gaussian peak with a FWHM of 0.09 Å^{-1}, punches of 3, 5, and 9 voxels (0.189 Å^{-1}, 0.315 Å^{-1}. 0.567 Å^{-1}, respectively) correspond to 95.3%, 99.98%, and 99.99999999995% absolute decays in signal, respectively. When considering integrated intensity, however, the 3, 5, and 9 voxel punches remove 98.7%, 99.996%, and essentially 100% of the total peak area, respectively. This suggests that a 3 voxel punch may leave some residual Bragg peak area, but the 5 and 9 voxel punches effectively remove all Bragg peaks at the estimated resolution.

2. Background

Background in an x-ray 3D-ΔPDF experiment typically contains any contribution from the sample environment and/or mounting apparatus, air scattering, and fluorescence and Compton scattering from the sample. To account for the background in our experiment, we measured 100 frames of an empty sample environment and averaged these. We then subtracted the averaged image of the empty sample environment from each image in a crystal rotation, pixel-wise, after normalizing both for exposure time. For comparison, we have carried out a reconstruction from detector to reciprocal space and full data processing (merging, symmetry averaging, punch and fill) both with and without this background subtraction. In Fig. S2 we show Q_x line scans of these two reciprocal space intensity distribution along the $Q_y = Q_z = 0$ Å^{-1} cut, along with the associated air scattering difference signal.

The air scattering signal is flat beyond $Q = \pm 5$ Å^{-1}. The measured intensity distribution after subtracting air scattering does appear to show a non-zero background contribution, but it is slowly varying with Q, and should contribute only a sinc type peak centered at the $\mathbf{r} = 0$ Å origin of direct space, and should not substantially alter features of interest.

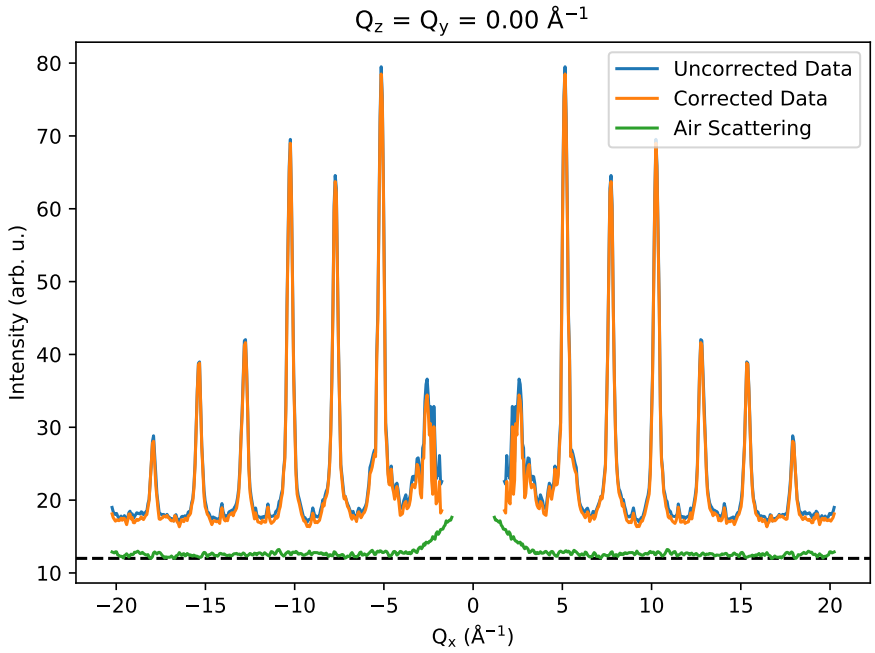

Fig. S2. A Q_x line scan of the reciprocal space intensity distribution at $Q_y = Q_z = 0$ Å^{-1}. The measured air scattering signal from an empty sample environment is shown, along with the reciprocal space intensity before and after subtraction of this air scattering signal. The air scattering signal has been shifted vertically for clarity, and the horizontal dashed line represents the shifted zero intensity point.

3. Symmetry Averaging

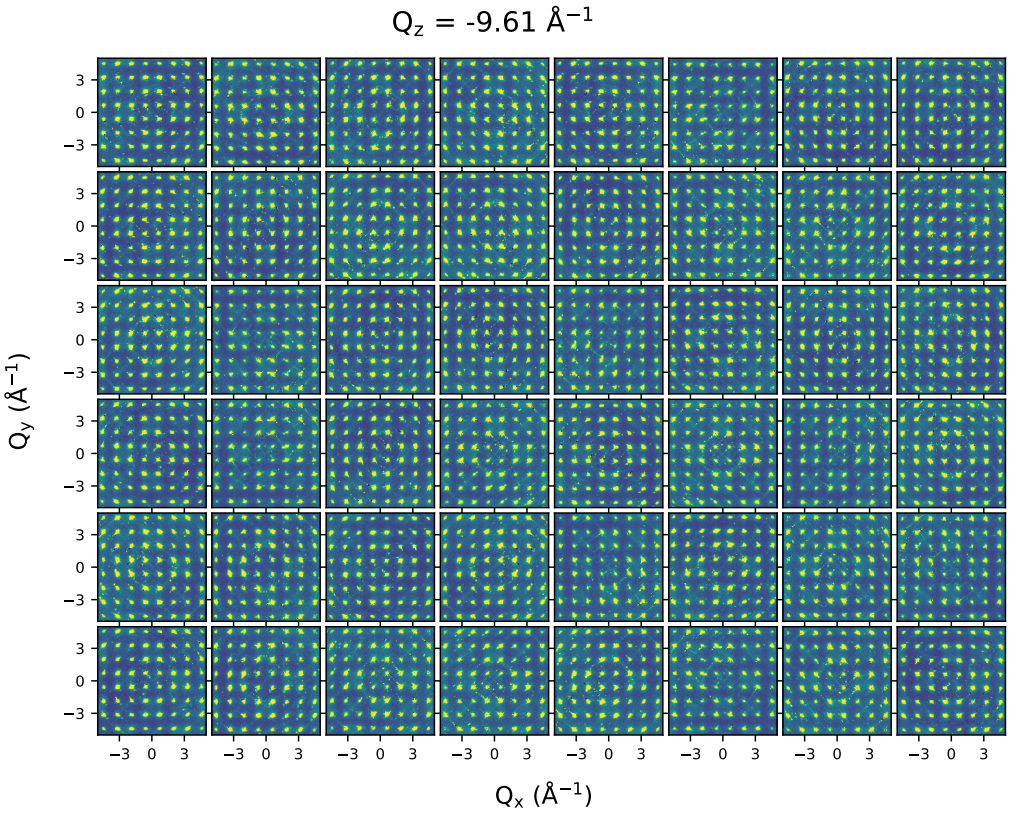

Fig. S3. Intensity distributions representing each of the 48 symmetry operations performed in symmetry averaging for this sample, at $Q_z = -9.61$ Å^{-1} over an abbreviated Q_x and Q_y range. The full averaging of these 48 intensity distributions is shown in Fig. S4(a), with explicit intensity bin histograms shown for three select voxels in Fig. S4(b-d).

Symmetry averaging involves merging symmetry equivalent transformations of the reciprocal space data. In the $CuIr_2S_4$ case explored here, 48 symmetry operations apply. Each panel of Fig. S3 shows a $Q_z = -9.61$ Å^{-1} slice of reciprocal space over an abbreviated Q_x and Q_y range after application of one of these 48 symmetry operations. Each of these symmetry operations contributes to the outlier-removed symmetry average, shown in panel Fig. S4(a). Three voxels are highlighted by colored circles in Fig. S4(a). Each of these circles (orange, brown, purple) corresponds respectively to

Fig. S4(b), (c), and (d), where the weighted intensity histograms are shown, and the associated Q_x and Q_y points are explicitly labeled. These histograms also include the weighted mean (dashed vertical black lines), two standard deviations from the weighted mean (dotted vertical red lines) and the outlier removed weighted mean (dashed vertical green lines).

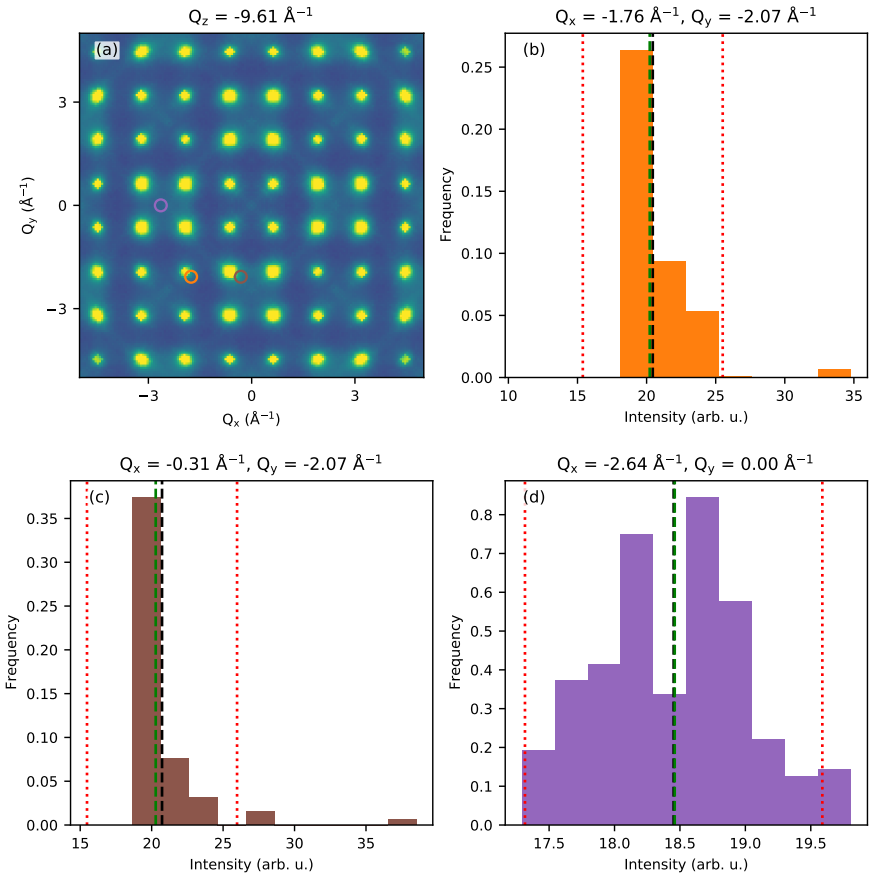

Fig. S4. (a) The full, outlier removed symmetry average of the 48 intensity distributions shown in Fig. S3, again at $Q_z = -9.61$ Å^{-1} over an abbreviated Q_x and Q_y range. Panels (b-d) show histograms of the intensity contributing to the highlighted voxels from each of the 48 intensity distributions in Fig. S3. Panel (b), (c), and (d) each correspond to the orange, brown, and purple circles, respectively, in panel (a), and each is labeled above the plot with the Q_x and Q_y of the corresponding voxel (all at $Q_z = -9.61$ Å^{-1}). In (b-d), the mean is shown by a vertical dashed black line, with ± two standard deviations depicted by vertical dotted red lines. The mean after excluding outliers is shown by a vertical dashed green line.

Voxels close to Bragg peaks (e.g. Fig. S4(b, c)) generally show narrow distributions

with a few small outliers at high intensity values, arising from detector artifacts. These outliers are successfully excluded by the process described in the main text. Voxels further from Bragg peaks (e.g. Fig. S4(d)) show very narrow distributions with nearly no outliers.

As has been stated in the main text, samples showing lower symmetry will contain fewer symmetry images, histograms akin to those shown in Fig. S4(b-d) will be sparser, and symmetry averaging may be less advantageous. This applies to situations where symmetry averaging aids in: correcting for detector artifacts, fills in portions of reciprocal space not sampled during the measurement, and/or replaces intensity excluded due to any masking procedure applied to the measured data. In such situations it may be necessary or advantageous to measure the crystal along multiple rotation axes to ensure that reciprocal space is properly sampled.

4. Reduced Q_{max}

To explore the role of Q_{max} in the data reduction process we have considered data over a smaller Q range. Specifically, Q_{max} has been chosen such that the entire voxel map contains measured data, effectively utilizing a cube which fits inside the sphere of $Q = 21$ Å^{-1}, or a cube where $|Q_x, Q_y, Q_z| \leq 15$ Å^{-1}. This can serve to simulate the effect of a reduced experimental Q_{max} as a result of using a lower x-ray beam energy, and/or a smaller/more distant detector. It additionally removes the hard boundary at $Q = 21$ Å^{-1} where intensity discontinuously falls off, as seen in the main text. A constant $Q_z = 0$ Å^{-1} slice of this truncated reciprocal space intensity distribution is shown in Fig. S5(a), and the the associated 3D-ΔPDF for this abbreviated Q-range is shown in Fig. S5(b). The effect on the 3D-ΔPDF is to substantially decrease the resolution, reducing each atom-pair feature to about 3 voxels on a side. This representation of the data is substantially less useful. Further, there is not a substantial

reduction of the Fourier ripples.

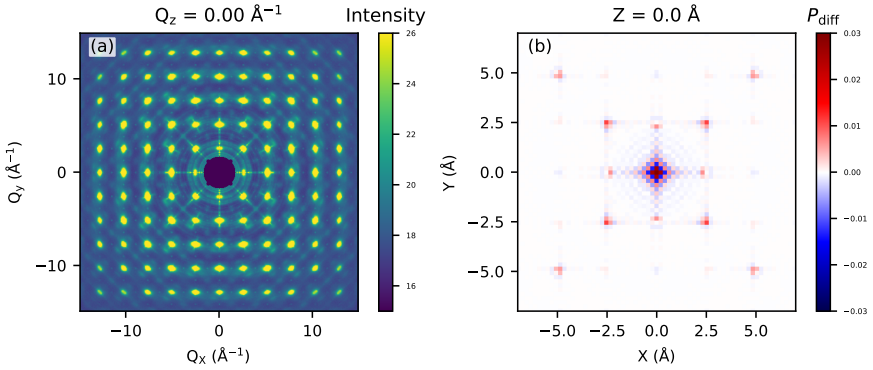

Fig. S5. (a) A $Q_z = 0$ Å^{-1} slice of the fully processed reciprocal space intensity distribution with an artificially low Q_{max}, where $|Q_x, Q_y, Q_z| \leq 15$ Å^{-1}. (b) A slice of the associated 3D-ΔPDF at $Z = 0$ Å resulting from the intensity distribution slice shown in (a).